2020

Influence of the Coriolis Effect on the Properties of Scattering Resonances in Symmetric and Asymmetric Isotopomers of Ozone

Igor Gayday
Marquette University

Elizaveta Grushnikova
Marquette University

Dmitri Babikov
Marquette University, dmitri.babikov@marquette.edu

Influence of The Coriolis Effect on The Properties of Scattering Resonances in Symmetric and Asymmetric Isotopomers Of Ozone

Igor Gayday
Department of Chemistry, Marquette University, Wehr Chemistry Building, Milwaukee, Wisconsin
Elizaveta Grushnikova
Department of Chemistry, Marquette University, Wehr Chemistry Building, Milwaukee, Wisconsin
Dmitri Babikov*
Department of Chemistry, Marquette University, Wehr Chemistry Building, Milwaukee, Wisconsin

Abstract

Scattering resonances above dissociation threshold are computed for four isotopically substituted ozone species: $^{16}O^{18}O^{16}O$, $^{16}O^{16}O^{18}O$, $^{18}O^{16}O^{18}O$ and $^{16}O^{18}O^{18}O$, using a variational method with accurate treatment of the rotation–vibration coupling terms (Coriolis effect) for all values of the total angular momentum J from 0 to 4. To make these calculations numerically affordable, a new approach was developed which employs one vibrational basis set optimized for a typical rotational excitation (J, Λ), to run coupled rotation–vibration calculations at several desired values of J. In order to quantify the effect of Coriolis coupling, new data are contrasted with those computed using the symmetric-top rotor approximation, where the rotation–vibration coupling terms are neglected. It is found that, overall, the major properties of scattering resonances (such as their lifetimes, the number of these states, and their cumulative partition function Q) are all influenced by the Coriolis effect and this influence grows as the angular momentum J is raised. However, it is found that the four isotopically substituted ozone molecules are affected roughly equally by the Coriolis coupling. When the ratio η of partition functions for asymmetric over symmetric ozone molecules is computed, the Coriolis effect largely cancels, and this cancelation seems to occur for all values of J. Therefore, it does not seem grounded to attribute any appreciable mass-independent symmetry-driven isotopic fractionation to the Coriolis coupling effect.

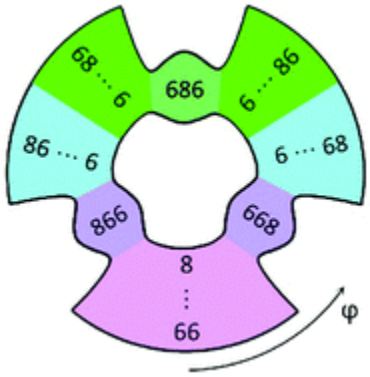

This article is part of the themed collection: 2020 PCCP HOT Articles

I. Introduction

An anomalous mass-independent fractionation in ozone isotopomers was first discovered almost 40 years ago by Mauersberger.[1] Ever since the discovery many research groups tried to explain the origin of this effect and countless papers have been published on this subject.[2–9] Despite the decades of intense work, the ultimate answer still remains a mystery and the ozone community is still looking for an answer to it.

In this manuscript we want to investigate a particular lead – a hypothesis proposed by Marcus and coworkers.[10,11] They suggested that some of the Coriolis coupling terms may be absent in the symmetric ozone molecules, but be present in the asymmetric ones, leading to a symmetry-driven (rather than mass-driven) isotope effect. In order to explore this possibility Marcus and co-workers carried out the classical trajectory simulations of the "diffusion" of vibrational excitations through the rotational states of symmetric and asymmetric ozone molecules. They found no isotope effect of this sort but concluded with the following statement: "*We speculate that the symmetry effect of Coriolis*

coupling can appear in quantum mechanical analysis of the model".[11] Therefore, it would be interesting to check this hypothesis, by doing rigorous quantum mechanical calculations, with all Hamiltonian terms responsible for the rotation–vibration coupling included, and with symmetry of the ro–vibrational wave functions taken into account.

Assessment of such a hypothesis is by no means trivial since considerable methodological and numerical effort is required to calculate the energies and lifetimes of scattering resonances above the dissociation threshold, let alone do the same for fully coupled rotational–vibrational states that take into account the effect of Coriolis coupling. Therefore this manuscript provides an important and novel contribution to the long-standing issue of isotope effects in ozone.

The effect of rotation–vibration coupling on the bound states of ozone (below the dissociation threshold) was studied in great detail, using both a semi-empirical model Hamiltonian,[12,13] and the first-principle calcualtions,[14,15] including two recent papers from our group.[16,17] There, we concluded that the observed effect of rotation–vibration coupling was not significantly different for symmetric and asymmetric isotopomers of ozone. This, however, might not hold true for the scattering resonances (above the dissociation threshold), whose properties are of much greater importance for the recombination reaction of ozone. Thus, in this manuscript we focus specifically on the properties of the scattering resonances.

Both scattering resonances and the effects of rotation–vibration coupling are computationally demanding in their own right, let alone when taken together. For this reason, the previous workers concerned with the scattering resonances in ozone,[18–23] did not take the rotation–vibration coupling into account. To the best of our knowledge, this article is the first to report and analyze the fully coupled rovibrational calculations of scattering resonances in $^{16}O^{18}O^{16}O$, $^{16}O^{16}O^{18}O$, $^{18}O^{16}O^{18}O$ and $^{16}O^{18}O^{18}O$, obtained entirely from the first-principle calculations.

Importantly, symmetric and asymmetric isotopomers of ozone (such as $^{16}O^{16}O^{18}O$ and $^{16}O^{18}O^{16}O$ in the case of single isotopic substitution) reside on a common global PES and should be addressed simultaneously, as two isomers of the same molecule that can interconvert at high energies. The first accurate calculations of this sort, with rotation–vibration coupling accurately included, were published very recently,[24] and were restricted to the relatively low vibrational excitation (about two quanta along each mode) and small values of the rotational quantum number, $J \leq 5$. More recently, we expanded the range of vibrational and rotational excitations considerably,[16] and extended these calculations onto the doubly substituted ozone molecule[17] (symmetric $^{18}O^{16}O^{18}O$ and asymmetric $^{16}O^{18}O^{18}O$ isotopomers), but we found that with a traditional (rotationally-adiabatic, see Section IIA) way of including the rotation–vibration coupling effect, implemented in the older version of our code (SpectrumSDT), it is impossible to reach scattering resonances above dissociation threshold. Numerically converged calculations of this sort happened to be computationally unaffordable for ozone isotopomers.

Here we present a modification of the original method that helps to carry out the coupled rotation–vibration calculations through the range of several values of the total angular momentum J in a more efficient way. A similar idea has been considered by Leforestier, but the theory has only been formulated for the case of Jacobi coordinates.[25] In the case of hyper-spherical coordinates, another

similar approach has been exploited in a context of the coupled-channel calculations of the reactive scattering,[26] but our approach is different, more efficient, and is applied here to reach the energy range above dissociation threshold (scattering resonances). Our method is presented in Sections II. In Section III this method and the new code are used to carry out the calculations of scattering resonances in singly and doubly substituted isotopologues of ozone, with accurate treatment of the rotation–vibration coupling: $^{16}O^{18}O^{16}O$, $^{16}O^{16}O^{18}O$, $^{18}O^{16}O^{18}O$ and $^{16}O^{18}O^{18}O$. Influence of the Coriolis effect on the properties of scattering resonances in symmetric and asymmetric ozone molecules, and its possible role in the symmetry driven mass-independent isotope effect, are discussed in Section IV. Conclusions are presented in Section V.

II. Theory

The general theoretical framework behind SpectrumSDT has been covered in detail in two recent publications,[16,17] where we studied the bound (stable) vibrational states of ozone and used a traditional rotationally-adiabatic basis set. In this section we present a concise summary of those derivations, discuss the advantages and disadvantages of this approach, and introduce modifications to make the calculations more efficient and capable of determining the properties of scattering resonances (the metastable states). Interested readers are encouraged to refer to references and for complete definitions of all notation used here.

A. Rotationally-adiabatic basis set

SpectrumSDT solves time-independent Schrodinger equation in adiabatically adjusting principal-axis hyper-spherical (APH) coordinates. These coordinates have been designed for 3-atomic systems and have 3 degrees of freedom: hyper-radius ρ (dissociative coordinate) and two hyper-angles θ and φ (non-dissociative vibrational coordinates). The rotational degrees of freedom are described using the conventional Euler angles α, β and γ.

As stated in reference, the Hamiltonian operator in APH coordinates can be expressed as (see Section A of ESI† for definition of the operators):

(1)

$$\widehat{H} = \hat{T}_\rho + \hat{T}_\vartheta + \hat{T}_\varphi + V_{\text{pes}} + V_{\text{ext}} + \hat{T}_{\text{sym}} + \hat{T}_{\text{asym}} + T_{\text{cor}},$$

with the corresponding matrix element given by:

(2)

$$\begin{aligned}\langle h_n X^j_{\Lambda n} \widetilde{D}_\Lambda \big| \widehat{H} \big| h_{n'} X^{j'}_{\Lambda' n'} \widetilde{D}_{\Lambda'} \rangle = {} & \langle h_n \big| \hat{T}_\rho \big| h_{n'} \rangle \langle X^j_{\Lambda n} \big| X^{j'}_{\Lambda n'} \rangle \tilde{\delta}_{\Lambda\Lambda'} \\ & + \langle X^j_{\Lambda n} \big| \hat{T}^n_\theta + \hat{T}^n_\varphi + V^n_{pes} + V^n_{ext} + V^{\Lambda n}_{rot} \big| X^{j'}_{\Lambda n} \rangle \delta_{nn'} \tilde{\delta}_{\Lambda\Lambda'} \\ & + \langle h_n X^j_{\Lambda n} \widetilde{D}_\Lambda \big| \hat{T}_{\text{asym}} + \hat{T}_{\text{cor}} \big| h_{n'} X^{j'}_{\Lambda' n'} \widetilde{D}_{\Lambda'} \rangle\end{aligned}$$

where the following basis set functions are used:

• $h_n(\rho)$ is an n-th DVR function along the ρ-grid;

• $X_{\Lambda n}^{j}(\theta,\phi)$ is a j -th 2D basis function in the hyper-angles θ and φ, optimized locally for ρ_n, and Λ is projection of the total angular momentum;

• $\widetilde{D}_{\Lambda}(\alpha,\beta,\gamma)$ is a modified Wigner function;

• $V_{rot}^{\Lambda n}$ is a rotational (centrifugal) potential derived from $\hat{T}_{sym}$ term in eqn (1).

The total angular momentum quantum number J is implicit in all our formula (not to be confused with the 2D basis function index j in $X_{\Lambda n}^{j}(\theta,\phi)$, introduced in the previous paragraph). The rotational potential $V_{rot}^{\Lambda n}(\theta)$ corresponds to a vibrating symmetric-top rotor and is given by

(3)

$$V_{\mathrm{rot}}^{\Lambda n}(\theta) = \hbar^2\left(J(J+1)\frac{A_n+B_n}{2} + \Lambda^2\left(C_n - \frac{A_n+B_n}{2}\right)\right)$$

where A_n, B_n and C_n are the values of rotational constants evaluated at $\rho = \rho_n$. Note that A_n and B_n enter eqn (3) only as their average.

In ref. 17, the basis functions $X_{\Lambda n}^{j}$ were defined as eigenfunctions of the 2D Hamiltonian:

(4)

$$\hat{H}_{\mathrm{2D}}^{\Lambda n} = \hat{T}_{\theta}^{n} + \hat{T}_{\varphi}^{n} + V_{\mathrm{pes}}^{n} + V_{\mathrm{ext}}^{n} + V_{\mathrm{rot}}^{\Lambda n},$$

(5)

$$\hat{\mathrm{H}}_{\mathrm{2D}}^{\Lambda n} X_{\Lambda n}^{j}(\theta,\varphi) = \varepsilon_{\Lambda n}^{j} X_{\Lambda n}^{j}(\theta,\varphi)$$

Note that with this definition $\hat{H}_{2D}^{\Lambda n}$ is different for each combination of J and Λ due to the rotational potential term $V_{\mathrm{rot}}^{\Lambda n}$. Such choice permits to take into account the effects of rotational excitation and distortion, by adjusting the 2D vibrational basis set $X_{\Lambda n}^{j}$ adiabatically, to be optimized specifically for each individual rotational state of the symmetric-top rotor (J,Λ). This requires solving the 2D vibrational problem $J+1$ times for each value of J, which by itself is not computationally demanding. The advantage of this elegant traditional approach is that we always operate with the most optimal basis set, which is expected to give the fastest convergence (with respect to the basis set size) and thus produce the smallest Hamiltonian matrix. The snag, however, is that one also needs to compute the overlap matrixes $\langle X_{\Lambda n}^{j} | X_{\Lambda' n'}^{j'} \rangle$ for each such set of solutions. The functions $X_{\Lambda n}^{j}$ are not analytical, so the overlaps have to be computed by explicit numerical integration and, for accurate calculations of the excited vibrational states or scattering resonances, the size of these matrices can be rather large. We found that in practice the computational cost of this integration outweighs considerably the advantage of having a slightly smaller Hamiltonian matrix.

B. Basis set of the non-rotating molecule $(J = 0)$

One way to circumvent this issue is to use the same set of 2D vibrational basis functions X_{n}^{j} for all values of J and Λ (note that index Λ, which we used to have in X_{n}^{j} before, does not appear anymore

since all functions X_n^j will have the same value of Λ here). One natural choice is to use basis functions obtained for the non-rotating molecule, $J = 0$ and $\Lambda = 0$, which has a simple physical motivation: the energy of rotational excitation (the "lift" of the potential energy surface (PES) that the molecule experiences as it rotates) is typically smaller than the vibrational energy of the molecule (the depth of the PES itself). Therefore, inclusion of the rotational excitation can be considered as a perturbation to the purely vibrational problem X_n^j, and the basis set optimized for a non-rotating molecule should in principle be suitable. The pay-off that one could foresee is that at large values of J the number of basis functions X_n^j, needed for convergence of results, may be higher compared to the rotationally-adiabatic choice of the basis.

The most straightforward way to define a basis set for non-rotating molecule is to simply move the rotational potential term out of the definition of $\widehat{H}_{2\mathrm{D}}^n$, so that eqn (4) becomes:

(6)

$$\widehat{H}_{2\mathrm{D}}^n = \hat{T}_\theta^n + \hat{T}_\varphi^n + V_{\mathrm{pes}}^n + V_{\mathrm{ext}}^n,$$

and eqn (2) becomes:

(7)

$$\begin{aligned}\langle h_n X_n^j \widetilde{D}_\Lambda \big| \widehat{H} \big| h_{n'} X_{n'}^{j'} \widetilde{D}_{\Lambda'} \rangle = {} & \langle h_n \big| \hat{T}_\rho \big| h_{n'} \rangle \langle X_n^j \big| X_{n'}^{j'} \rangle \tilde{\delta}_{\Lambda\Lambda'} \\ & + \langle X_n^j \big| \widehat{H}_{2\mathrm{D}}^n \big| X_n^{j'} \rangle \delta_{nn'} \tilde{\delta}_{\Lambda\Lambda'} + \langle X_n^j \big| V_{\mathrm{rot}}^{\Lambda n} \big| X_n^{j'} \rangle \delta_{nn'} \tilde{\delta}_{\Lambda\Lambda'} \\ & \langle h_n X_n^j \widetilde{D}_\Lambda \big| \hat{T}_{\mathrm{asym}} + \hat{T}_{\mathrm{cor}} \big| h_{n'} X_{n'}^{j'} \widetilde{D}_{\Lambda'} \rangle\end{aligned}$$

For the symmetric-top rotor term we obtain (following the derivations in ref. 16 and 17):

(8)

$$\langle X_n^j \big| V_{\mathrm{rot}}^{\Lambda n} \big| X_n^{j'} \rangle = \hbar^2 \left(J(J+1) \langle X_n^j \left| \frac{A_n + B_n}{2} \right| X_n^{j'} \rangle + \Lambda^2 \langle X_n^j \left| C_n \frac{A_n + B_n}{2} \right| X_n^{j'} \rangle \right)$$

Note, that the matrix of eqn (8) is diagonal in n and Λ due to the $\delta_{nn'}\tilde{\delta}_{\Lambda\Lambda'}$ factor in eqn (7). The asymmetric-top rotor term $\hat{T}_{asym}$ and the Coriolis term $\hat{T}_{cor}$ are treated as before.

C. Basis set of a rotationally excited molecule (arbitrary J, Λ)

The basis set X_n^j of the non-rotating molecule (J, Λ) = (0,0) can be efficient and sufficient for the ro–vibrational calculations at small values of J. However, for prediction of thermal reaction rates at room temperature one often has to deal with rotational states up to $J_{\max} \sim 100$. For ozone recombination reaction in particular, the calculations of rotational states up to $J_{\max} \sim 50$ are desirable. If the calculations for all these values of J and Λ are to be carried out with the same basis set, it would certainly make more sense to choose one that corresponds to the values of J and Λ somewhere in the middle of the broad range of rotational excitations.

Let's say that we optimized one basis set X_n^j for a chosen pair of $(J, \Lambda) = (J_{\mathrm{bs}}, \Lambda_{\mathrm{bs}})$, picked somewhere in the range $0 \leq J_{\mathrm{bs}} \leq J_{\max}$ and $0 \leq \Lambda_{\mathrm{bs}} \leq J_{\mathrm{bs}}$ based on physical intuition, energy considerations, or some kind of a convergence study. Subscript "bs" denotes the values of J and Λ native to this basis set. The corresponding value of the vibrating symmetric-top rotor energy $V_{\mathrm{rot}}^{\Lambda}$ will be denoted as $V_{\mathrm{rot}}^{\mathrm{bs}}$. In order to employ such basis set in the ro–vibrational calculations for an arbitrary J, with all $0 \leq \Lambda \leq$ J included, we simply add $V_{\mathrm{rot}}^{\mathrm{bs}}$ to eqn (6) and subtract it from the symmetric-top rotor term in eqn (7). The resultant two formula are:

(9)

$$\widehat{H}_{\mathrm{2D}}^{\mathrm{n}} = \hat{T}_{\theta}^{\mathrm{n}} + \hat{T}_{\phi}^{\mathrm{n}} + V_{\mathrm{pes}}^{\mathrm{n}} + V_{\mathrm{ext}}^{\mathrm{n}} + \mathrm{V}_{\mathrm{rot}}^{\mathrm{bs,n}},$$

$$\begin{aligned}\langle h_n X_n^j \widetilde{D}_{\Lambda} | \widehat{H} | h_{n'} X_{n'}^{j'} \widetilde{D}_{\Lambda'} \rangle &= \langle h_n | \hat{T}_{\rho} | h_{n'} \rangle \langle X_n^j | X_{n'}^{j'} \rangle \tilde{\delta}_{\Lambda\Lambda'} \\ &+ \langle X_n^j | \widehat{H}_{2D}^n | X_n^{j'} \rangle \delta_{nn'} \tilde{\delta}_{\Lambda\Lambda'} + \langle X_n^j | V_{\mathrm{rot}}^{\Lambda n} \\ &- V_{\mathrm{rot}}^{\mathrm{bs},n} | X_{n'}^{j'} \rangle \delta_{nn'} \tilde{\delta}_{\Lambda\Lambda'} + \langle h_n X_n^j \widetilde{D}_{\Lambda} | \hat{T}_{\mathrm{asym}} \\ &+ \hat{T}_{\mathrm{cor}} | h_{n'} X_{n'}^{j'} \widetilde{D}_{\Lambda'} \rangle\end{aligned}$$

(10)

The goal of this swap of terms in the overall Hamiltonian is to compensate for the centrifugal lift of the chosen basis set, permitting to predict ro–vibrational energies for any rotational excitation J, which can be both smaller ($J < J_{\mathrm{bs}}$) or larger ($J \geq J_{\mathrm{bs}}$) than that of the chosen basis set.

Incorporating these results into the final expression for the Hamiltonian matrix element in terms of the expansion coefficients of 1D (a_{nlm}^i) and 2D (b_{nli}^j) basis functions we obtain:

$$
\begin{aligned}
\langle h_n X_n^j \widetilde{D}_\Lambda \big| \widehat{H} \big| h_{n'} X_{n'}^{j'} \widetilde{D}_{\Lambda'} \rangle \quad &= \tilde{\delta}_{\Lambda\Lambda'} \left(\langle h_n \big| \hat{T}_\rho \big| h_{n'} \rangle \sum_l^L \sum_m^M \left(\sum_i^{S_{nl}} b_{nli}^j a_{nlm}^i \right) \times \left(\sum_{i'}^{S_{n'l}} b_{n'li'}^{j'} a_{n'lm}^{j'} \right) \delta_{nn'} \delta_{jj'} \varepsilon_n^j \right) \\
&+ \frac{-h^2}{4} U_{\Lambda\Lambda'} \delta_{nn'} \sum_l^L (A_{nl} - B_{nl}) \\
&\times \sum_m^M \left(\sum_i^{S_{nl}} b_{nli}^j a_{nlm}^i \right) \left(\sum_i^{S_{nl}} b_{nli'}^{j'} a_{nlm}^{i'} \right) \\
&+ (-1)^{\Lambda+s} 2\hbar^2 W_{\Lambda\Lambda'} \delta_{nn'} \sum_l^L B_{nl} \cos\theta_l \\
&\times \sum_m^M m \left(\sum_i^{S_{nl}} b_{nli}^j a_{nlm}^i \right) \left(\sum_{i'}^{S_{nl}} b_{nli'}^{j'} a_{nlm}^{i'} \right) \\
&+ \tilde{\delta}_{\Lambda\Lambda'} \delta_{nn'} \hbar^2 \cdot \left(\left(\frac{J(J+1) - J_{\mathrm{bs}}(J_{\mathrm{bs}}+1)}{2} \right) \right. \\
&\times \sum_l^L (A_{nl} - B_{nl}) \sum_m^M \left(\sum_i^{S_{nl}} b_{nli}^j a_{nlm}^i \right) \\
&\times \left(\sum_{i'}^{S_{nl}} b_{nli'}^{j'} a_{nlm}^{i'} \right) \\
&+ \left(\Lambda^2 - {\Lambda_{\mathrm{bs}}}^2 \right) \sum_l^L \left(C_{nl} - \frac{A_{nl} + B_{nl}}{2} \right) \\
&\left. \times \sum_m^M \left(\sum_i^{S_{nl}} b_{nli}^j a_{nlm}^i \right) \left(\sum_{i'}^{S_{nl}} b_{nli'}^{j'} a_{nlm}^{i'} \right) \right)
\end{aligned}
$$

(11)

where L is the total number of DVR functions in the basis set for coordinate θ, M is the total number of VBR functions for coordinate φ, S_{nl} is the total number of 1D solutions at $\rho = \rho_n$ and $\theta = \theta_l$, and matrices $U_{\Lambda\Lambda'}$ and $W_{\Lambda\Lambda'}$ quantify the strength of asymmetric top rotor and Coriolis coupling terms. See ref. 17 for exact definitions and further details.

D. Tests of the new basis set approach

We implemented this new choice of the basis set in the SpectrumSDT program and rigorously tested it, by re-doing the bound state calculations reported earlier[16,17] for $0 \leq J \leq 5$ and expanding the range of rotational excitations significantly, up to $J = 56$.

To quantify the accuracy of our approach we calculated vibrational energy levels for a selected rotational state $(J, \Lambda) = (56,2)$ using two basis sets: a local basis set, optimized for the same values of $(J, \Lambda) = (56,2)$ (about 20 000 basis functions), and a basis set chosen in the middle of the range with $(J, \Lambda) = (24,2)$ (about 22 000 basis functions). In each case the energies of 1000 vibrational states in a broad energy range (from the bottom of the well up to 600 cm^{-1} above the dissociation threshold) were calculated The differences between energies predicted by these two calculations start at $\sim 10^{-6}$ cm^{-1} for the bound states near the bottom of the well, and gradually increase up to ~ 1 cm^{-1} for resonances above the dissociation threshold. Such differences are within our target convergence and can be further reduced by increasing the basis set size, if necessary. Therefore we conclude that our approach is reliable and accurate.

The computational speed up, due to no need to integrate the overlaps $\langle X^{j}_{\Lambda n} | X^{j'}_{\Lambda' n'} \rangle$ for all values of Λ and J anymore, was found to be very substantial. This new feature permitted us to climb higher in energy, up to the dissociation threshold and above, to access the range of scattering resonances for rovibrational states.

III. Results

A. Distributions of state properties

The methodology described above was utilized to compute all coupled rotational–vibrational states of singly and doubly substituted ozone molecules up to the energy of 1000 cm^{-1} above the dissociation threshold for five values of the total angular momentum $0 \leq J \leq 4$ and with all values of Λ included. The reference basis set X^{j}_{n} was optimized for $J = 4$ and $\Lambda = 2$. Only the states with positive energy (scattering resonances above dissociation threshold) were considered in the following analysis (around 80 000 states total). SpectrumSDT uses SLEPc library to find these eigenstates.[27–29] A complex absorbing potential (CAP) in the form suggested by Manolopoulos[30] was used to impose the boundary conditions. The CAP was defined with the minimum absorption energy $E_{\min}$ = 7 cm^{-1} and spans the range of ~6 Bohr from the end of the ρ-grid. All other technical details of our calculations are outlined in the ESI.†

There are two potential energy surfaces for ozone currently in use: DLLJG[31] and TKTHS.[32] As evidenced by Fig. 6 of ref. 33, both DLLJG and TKTHS surfaces lead to comparable errors relative to the experimental results. In this manuscript we decided to continue with DLLJG surface.

For every resonance we computed its energy E_i and width Γ_i, which determines its lifetime through $\tau_i = \hbar/\Gamma_i$, and the decay rate $k_i = \Gamma_i/\hbar$. It is nearly impossible to converge every individual state above the dissociation threshold. Therefore, our convergence parameters, including position of the CAP, were adjusted to ensure convergence of the overall partition function of the molecule (Q, defined in eqn (12)) to within 1%. Convergence of the individual states depends on their properties. Broad resonances with $\Gamma \sim 10$ cm^{-1} are converged to within 1 cm^{-1} or better (both energy and width). Narrower resonances are converged much better. Convergence of broader resonances is not important, since they make negligibly small contributions to the dynamical partition function Q (their weights w_i are close to 1, but their probabilities p_i are close to 0, see eqn (13) below).

Moreover, in order to have more information about the nature of each state, we integrated the modulus squared of its wavefunction over five specific regions of the PES, indicated by color in Fig. 1. The resultant five probabilities are listed in Table 1 for the case of singly substituted ozone molecule. The case of doubly substituted ozone molecule is analyzed similarly and is covered in the ESI.†

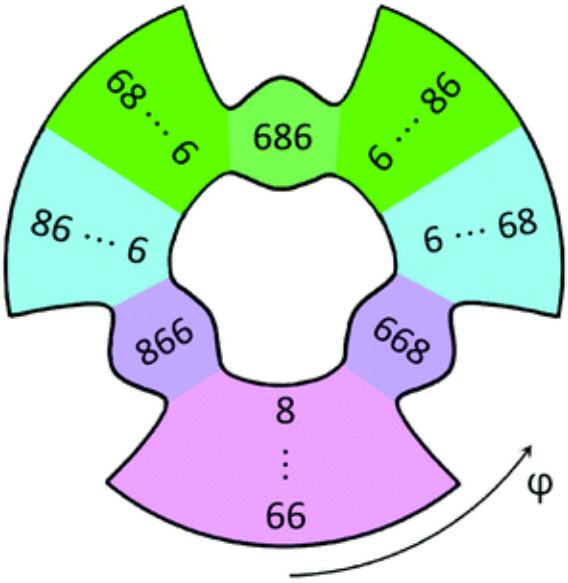

Fig. 1 A schematic representation of the PES of ozone, labelled for the case of a singly substituted molecule. Three tight deep wells correspond to the covalently bound ozone molecules: $^{16}O^{18}O^{16}O$ (single well) and $^{16}O^{16}O^{18}O$ (double well). Five broad and shallow plateaus correspond to the weakly bound van der Waals complexes: $^{16}O^{18}O\cdots^{16}O$, $^{16}O^{16}O\cdots^{18}O$ and $^{16}O\cdots^{16}O^{18}O$ (double-well each). The meaning of colors is summarized in Table 1. The arrow shows direction of change of φ-coordinate.

Table 1 Definitions of five probabilities computed for each ro-vibrational state of ozone

Color in Fig. 1	**Meaning**	**Probability**
Green	Covalently bound symmetric ozone molecule $^{16}O^{18}O^{16}O$	p_i^{SYM}
Purple	Covalently bound asymmetric ozone molecules $^{16}O^{16}O^{18}O$	p_i^{ASYM}
Light blue	van der Waals complex in the ^{16}O + $^{16}O^{18}O$ channel, near asymmetric $^{16}O^{16}O^{18}O$	$p_i^{\mathrm{vdW(A)}}$
Light green	van der Waals complex in the $^{16}O^{18}O$ + ^{16}O channel, near symmetric $^{16}O^{18}O^{16}O$	$p_i^{\mathrm{vdW(S)}}$
Pink	van der Waals complexes in the $^{16}O^{16}O$ + ^{18}O channel	$p_i^{\mathrm{vdW(B)}}$

Note that vdW(A) is separated from vdW(S) by the potential energy barrier on the PES. The corresponding isomers do not interconvert freely, and therefore should both be defined and included into consideration separately. This is particularly important since one of them is associated with symmetric, while the other one with asymmetric ozone molecule, even though asymptotically they both merge into a single dissociation channel. This is further discussed in the next section. Additional details can be found in the ESI.†

We found that the complexity of the PES of ozone is responsible for the appearance of a broad distribution of properties of its states. An overview is presented in Fig. 2, where each point corresponds to one computed ro–vibrational state. Two axes give the total covalent ($p_i^{\mathrm{SYM}} + p_i^{\mathrm{ASYM}}$) and total van der Waals ($p_i^{\mathrm{vdW(A)}} + p_i^{\mathrm{vdW(B)}} + p_i^{\mathrm{vdW(S)}}$) probabilities. Color in Fig. 2 reflects the value of Γ_i (on a log scale).

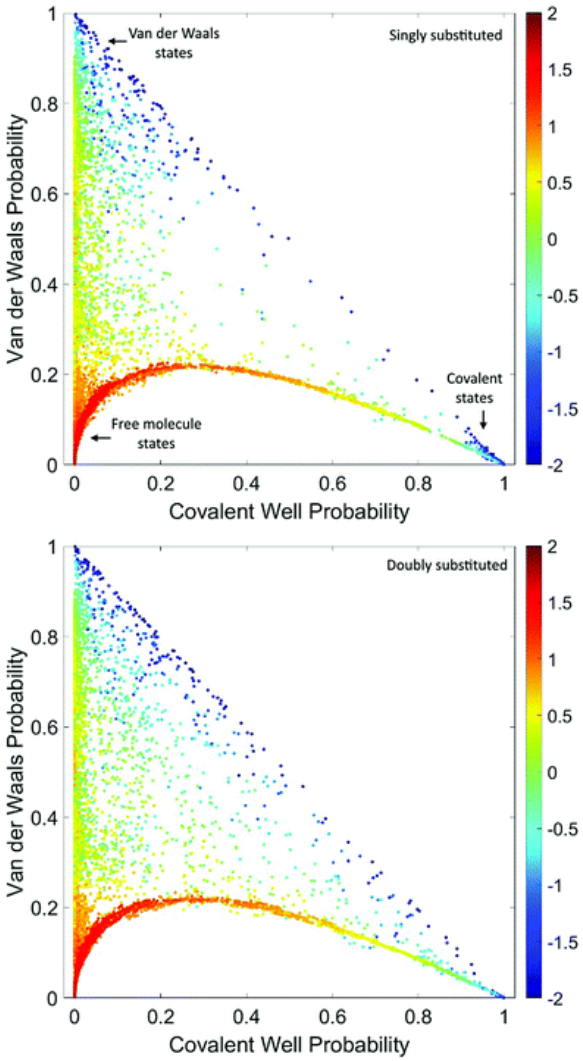

Fig. 2 Distribution of the covalent and van der Waals probabilities for scattering resonances in the singly substituted (upper frame) and doubly substituted (lower frame) molecules of ozone, based on the coupled ro–vibrational calculations up to $J = 4$. Color corresponds to the resonance width, on a logarithmic scale (see text).

From Fig. 2 we can see that both singly and doubly substituted ozone molecules exhibit broad distributions of state properties. The lower right corner of each frame corresponds to the mainly covalent states, while the upper left corner corresponds to the mainly van der Waals (vdW) states, and we see that both kinds of resonance states are possible in ozone.

The five probabilities defined in Table 1 and used to plot Fig. 2 correspond to contiguous regions on the PES, so, whenever they do not add up to 1, the remaining probability corresponds to the asymptotic

part of the PES (dissociation channels). Qualitatively, the more a point deviates from the diagonal in Fig. 2, the more probability in the dissociation region it has. In particular, the points near the origin have all their probability in the dissociation region and correspond to the continuum of free particle states, while the points on the diagonal have no probability in the dissociation region and correspond to the bound states.

Another feature of Fig. 2 is a high density of points along the vertical axis, which means that most states tend to have higher probability in vdW or asymptotic regions and only relatively small number of states can feature high probability in the covalent regions. The fact that this density is relatively uniform tells us that the states with negligible covalent character are almost equally likely to be any combination of vdW and free molecule states.

Finally, note the absence of any states along the horizontal axis in Fig. 2. Any hypothetical state there would need to have significant probabilities in the covalent and dissociation regions, while having zero probability in the vdW region. The covalent and dissociation regions are separated by vdW region, so it comes as no surprise that all the actual states that have non-zero probability in covalent and dissociation regions simultaneously, also have non-zero probability in vdW region.

Tracking the points from right to left along the edge of this empty area in the right half of the plot, one can see that any probability "missing" from the covalent region gets redistributed between vdW and dissociation regions rather uniformly, taking into account that the dissociation region is about 60% larger than vdW. The same does not hold true in the left half of the plot, where the points along the edge start having more probability in the dissociation region compared to the vdW region.

The typical values of resonance widths vary through four orders of magnitude range, $10^{-2} \leq \Gamma_i \leq 10^{2}\ \mathrm{cm}^{-1}$. Narrower (longer lived) states are shown by blue points in Fig. 2, and are found mainly in the covalent corner, in the vdW corner, and along the diagonal line that connects them. They correspond to the relatively stable states, not coupled to the asymptotic region of free particle states, which explains their stability. Broader (short lived) states are shown by red points in Fig. 2, and are found mainly near the origin, which corresponds to the mostly free-particle states, which also makes sense. Note that the states with substantial vdW probability (around 0.5) appear to be longer-lived (they have smaller gammas) than the states with the same probabilities in the covalent region.

B. Average properties of scattering resonances

Since different resonances exhibit rather different properties, it is useful to average those over the distribution, in order to obtain a small set of representative values (which can be used for comparison of different isotopomers of ozone, for example). In order to be meaningful, this should be a weighted average that takes into account the importance of a given scattering resonance in the ozone recombination reaction. Building upon the previous work,[23] we define the weight of each state i in the average as its contribution to the corresponding partition function:

$$Q_i = p_i w_i \exp\left(-\frac{E_i}{kT}\right) \tag{12}$$

In what follows, the average values will be computed separately for the covalent and the vdW states, for symmetric and asymmetric ozone isotopomers, and for the singly and doubly substituted ozone isotopologues. Therefore, the first factor in eqn (12) is introduced to take that into account and corresponds to the state's probability p_i associated with a given region on the PES, as defined in Table 1.

The second factor in eqn (12) is a weight w_i:

$$w_i = \frac{\Gamma_i/\hbar}{\Gamma_i/\hbar + [\mathrm{M}]k_i^{\mathrm{stab}}}$$

(13)

This weight is based on the standard Lindeman mechanism of recombination and accounts for state population at a given pressure of bath gas, which lets one to give higher weights to wider states that are naturally more important for the recombination reaction. The lower the pressure, the less restrictive this factor is. For example, in the limit of zero pressure, all states would be equally important regardless of their widths. For stabilization rate coefficient k_i^{stab}, we use a simple model introduced previously[23] (see also ESI† for more details).

The last thing in eqn (12) is the Boltzmann factor at given temperature. Here and further in the text we assume the conditions that correspond to the experiments of Mauersberger group with $[\mathrm{M}] = 0.3$ Bar and $T = 298$ K.[34]

All three factors in eqn (12) vary between zero and one, so the value of Q_i is also less than one. Importantly, the sum of Q_i over the states of a given molecule represents its dynamical partition function:[23] $Q = \sum Q_i$. The "dynamical" prefix here is used to stress that it depends on dynamical factors, such as lifetime of the states, as well as on pressure and temperature. It is important to take into account these factors since they play a crucial role in the ozone recombination reactions.

Note that here we report the values of vibrational partition functions Q per rotational state (of a symmetric top rotor, *i.e.* divided by the number of rotational Λ-blocks in the ro–vibrational calculation). Additionally, the values of Q for asymmetric ozone isotopomers are divided by 2, to account for the number of wells and put all partition functions values in Table 2 on the same scale.

Table 2 Average properties of scattering resonances in the covalent wells of ozone, computed for various isotopic substitutions based on the coupled ro–vibrational calculations up to $J = 4$. The data in parentheses correspond to the approximate symmetric-top rotor treatment

	$^{16}O^{18}O^{16}O$	$^{16}O^{16}O^{18}O$	$^{18}O^{16}O^{18}O$	$^{16}O^{18}O^{18}O$
$\tilde{\Gamma}$, cm^{-1}	3.12 (3.19)	3.29 (3.36)	2.06 (2.14)	3.05 (3.16)
Q	4.66 (4.53)	4.54 (4.41)	5.86 (5.65)	5.12 (4.93)
$\tilde{p}$	0.532 (0.552)	0.528 (0.541)	0.575 (0.600)	0.499 (0.522)
$\tilde{Q}_i$	0.230 (0.242)	0.241(0.245)	0.254 (0.266)	0.238 (0.248)
$\tilde{N}$	20.4 (18.9)	18.8 (18.0)	23.1 (21.3)	21.5 (20.0)
η	0.975 (0.974)		0.874 (0.873)	

The first row of Tables 2–4 lists all possible isotopic substitutions, and the main question here is how the symmetric and asymmetric ozone molecules compare and contrast. In the second row of Tables 2–4 we report the weighted average values of the resonance width, computed as $\tilde{\Gamma} = \sum Q_i \Gamma_i / Q$, for the covalent ozone states (Table 2), for the vdW complexes (Table 3), and for all these states taken together (Table 4). The partition functions Q for the same cases are reported in the third row of Tables 2–4. Rows 3 to 6 report several other weighted average properties: the average wavefunction probability $\tilde{p} = \sum Q_i p_i / Q$; the average contribution of one resonance to the partition function $\tilde{Q}_i = \sum Q_i Q_i / Q$; and the average "number of resonances" $\tilde{N} = Q/Q_i$. Note, that $\tilde{N}$ is not literally a number of resonances, but rather a factor relating Q and $\tilde{Q}_i$, which can be roughly thought of as a "number of resonances" (and such terminology will be used in this paper), but one should still be careful with its interpretation. Finally, the last row of Tables 2 and 4 gives the value of η-effect, defined as $\eta = Q(^{16}O^{16}O^{18}O)/Q(^{16}O^{18}O^{16}O)$ for single substitution, and $\eta = Q(^{16}O^{18}O^{18}O)/Q(^{18}O^{16}O^{18}O)$ for double substitution.

Table 3 Average properties of scattering resonances in the van der Waals plateaus of ozone, computed for various isotopic substitutions based on the coupled ro–vibrational calculations up to $J = 4$. The data in parentheses correspond to the approximate symmetric-top rotor treatment

	^{16}O^{16}O…^{18}O	**^{16}O…^{16}O^{18}O and ^{16}O^{18}O…^{16}O**	**^{16}O…^{18}O^{18}O**	**^{16}O^{18}O…^{18}O and ^{18}O^{16}O…^{18}O**
$\tilde{\Gamma}$, cm^{-1}	6.01 (6.10)	7.20 (7.25)	7.03 (7.18)	6.12 (6.19)
Q	17.1 (16.7)	17.0 (16.7)	18.2 (17.7)	17.7 (17.4)
$\tilde{p}$	0.458 (0.473)	0.397 (0.408)	0.346 (0.360)	0.427 (0.443)
$\tilde{Q}_i$	0.299 (0.304)	0.270 (0.275)	0.224 (0.230)	0.275 (0.282)
$\tilde{N}$	57 (55.1)	63.4 (61.2)	81.6 (77.6)	64.5 (61.7)

Table 4 Average properties of all scattering resonances in ozone, computed for various isotopic substitutions based on the coupled ro–vibrational calculations up to $J = 4$. The data in parentheses correspond to the approximate symmetric-top rotor treatment

	^{16}O^{18}O^{16}O	**^{16}O^{16}O^{18}O**	**^{18}O^{16}O^{18}O**	**^{16}O^{18}O^{18}O**
$\tilde{\Gamma}$, cm^{-1}	6.24 (6.30)	5.95 (6.02)	5.04 (5.12)	5.83 (5.95)
Q	21.8 (21.3)	21.6 (21.1)	23.2 (22.7)	23.3 (22.6)
$\tilde{p}$	0.328 (0.333)	0.451 (0.455)	0.366 (0.374)	0.430 (0.431)
$\tilde{Q}_i$	0.192 (0.194)	0.278 (0.274)	0.207 (0.210)	0.266 (0.260)
$\tilde{N}$	114 (111)	77.7 (77.0)	112 (109)	87.7 (87.1)
η	0.991 (0.992)		1.00 (0.999)	

For ozone resonances localized over the covalent well we found that average values $\tilde{\Gamma}$ in asymmetric ozone molecules are larger than those in symmetric ones, by 5.5% in the case of single and by as much as 48% in the case of double substitution (see Table 2). We attribute it to the fact that the well on the PES that hosts the symmetric ozone molecule (see Fig. 1), and the vibrational wavefunctions that sit in this well, are always symmetric with respect to the well's dissociation channels (^{16}O + ^{18}O^{16}O and ^{16}O^{18}O + ^{16}O in Fig. 1). Each such wavefunction must decay equally into these channels. In contrast, the double-wells on the PES that host asymmetric ozone molecules (see Fig. 1) are slightly tilted, which

introduces asymmetry into the vibrational wavefunctions. Some of these states lean more towards one channel (say $^{16}O + {}^{16}O^{18}O$) and dissociate primarily into it, while other states lean more towards and dissociate primarily into the other channel ($^{16}O^{16}O + {}^{18}O$). Overall, such asymmetric dissociation appears to be more efficient, and this is observed for the states localized over the covalent wells in both singly and doubly substituted molecules. Therefore the "driving force" of this effect is symmetry, not the mass.

Interestingly, scattering resonances distributed over the vdW plateau of the PES behave differently. In the case of single isotopic substitution, the vdW states in the asymmetric channel ($^{16}O + {}^{16}O^{18}O$) exhibit larger values of $\tilde{\Gamma}$ than those in the symmetric channel ($^{16}O^{16}O + {}^{18}O$) by 20%. But in the case of double substitution the picture is reversed and the vdW states in the asymmetric channel ($^{16}O^{18}O + {}^{18}O$) exhibit smaller values of $\tilde{\Gamma}$ than those in the symmetric channel ($^{16}O + {}^{18}O^{18}O$) by 13%. Explanation for this "flip" is that the vdW states, located in the channel region of the PES, are primarily influenced by the value of asymptotic vibrational zero-point energy (ZPE) of the channel. In the case of single substitution the asymmetric channel is deeper, because ZPE($^{16}O^{18}O$) < ZPE($^{16}O^{16}O$), but in the case of double substitution the symmetric channel is deeper, because ZPE($^{16}O^{18}O$) > ZPE($^{18}O^{18}O$). The decay of resonances into a deeper channel is always more efficient, and therefore for the vdW states the "driving force" of the effect is the mass, rather than symmetry.

Comparing Tables 2 and 3 one notices that the values of $\tilde{\Gamma}$ for vdW states are much larger than those for the covalent states, by a factor of ×2 to ×3. This makes sense, since resonances located in the longer-range part of the PES are expected to decay faster. This might seem to contradict the results in Fig. 2, but keep in mind that the weight function in eqn (12) favors certain states more than others, which makes the direct estimation of these quantities from Fig. 2 non-trivial. Also from Tables 2 and 3, one can clearly see that the partition functions Q of resonances distributed over the vdW parts of the PES are significantly larger than those of the resonances localized over the covalent wells, by a factor of ×3 to ×4.

At present time it is not entirely clear what is the role of the vdW states of ozone in the recombination process,[20,35,36] but here, as a limiting case, we will compute the average values for resonances of both kinds put together. This is presented in Table 4, where the vdW states in the symmetric channel ($^{16}O^{16}O\cdots{}^{18}O$ in Fig. 1 for single substitution) are said to contribute to the asymmetric molecule $^{16}O^{16}O^{18}O$, while the vdW states in the asymmetric channel are split: the vdW states $^{16}O\cdots{}^{16}O^{18}O$ are said contribute to the asymmetric ozone $^{16}O^{16}O^{18}O$, while the vdW states $^{16}O\cdots{}^{18}O^{16}O$ are said contribute to the symmetric ozone $^{16}O^{18}O^{16}O$. Using Table 1 the corresponding probabilities used in eqn (12) are $p_i^{\mathrm{SYM}} + p_i^{\mathrm{vdW(S)}}$ for symmetric and $p_i^{\mathrm{ASYM}} + p_i^{\mathrm{vdW(A)}} + p_i^{\mathrm{vdW(B)}}$ for asymmetric ozone molecules. And similar for the case of double substitution.

From Table 4 one can clearly see that when the covalent and the vdW resonances are both accounted, the values of partition functions Q for symmetric and asymmetric ozone species e$q$ualize (to within less than 1% difference), in both singly and doubly substituted cases. It was not the case when only the covalent well probabilities were included into Q. Indeed, in Table 2 asymmetric ozone molecules exhibit smaller Q than the symmetric molecules, by 3% and 13% in the cases of single and double

substitutions, respectively. As for the values of average resonance width $\tilde{\Gamma}$, the mass-effect driven by ZPE (brought about by the vdW states) dominates. Namely, in Table 4, in the singly substituted case the values of $\tilde{\Gamma}$ for asymmetric molecules are smaller by 5% than those for symmetric molecules, but this is opposite in the doubly substituted case where the values of $\tilde{\Gamma}$ for asymmetric molecules are larger by 15%.

C. Influence of the rotational excitation

The values of resonance widths Γ_i and their contributions to the partition function Q_i do depend on the rotational excitation J, but not dramatically. In Fig. 3 and 4a we reported $Q(J)$ and $\tilde{\Gamma}(J)$ dependencies, obtained as weighted averages of the vibrational states for each value of J, with both covalent and vdW resonances included. The largest change is observed for going from $J = 0$ to $J = 1$, after which both dependencies evolve slower and rather monotonic. The dependencies $Q(J)$ and $\tilde{\Gamma}(J)$ computed for the covalent states and for the vdW states separately can be found in the Fig. S2, S4a, S5 and S7a, respectively, in the ESI.†

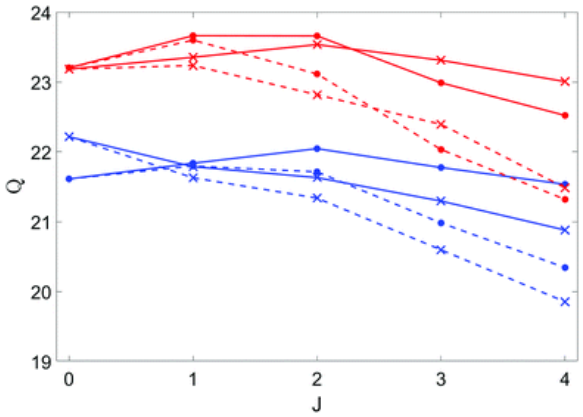

Fig. 3 Partition function Q of scattering resonances in ozone as a function of rotational excitation up to $J = 4$. The states localized over the covalent well, and those distributed over the van der Waals region of the PES, are both included. The blue (red) color corresponds to the singly (doubly) substituted isotopologues of ozone. The dots (x-symbols) correspond to symmetric (asymmetric) isotopomers. The solid (dashed) lines correspond to the accurate coupled rotation–vibration (approximate symmetric-top rotor) calculations.

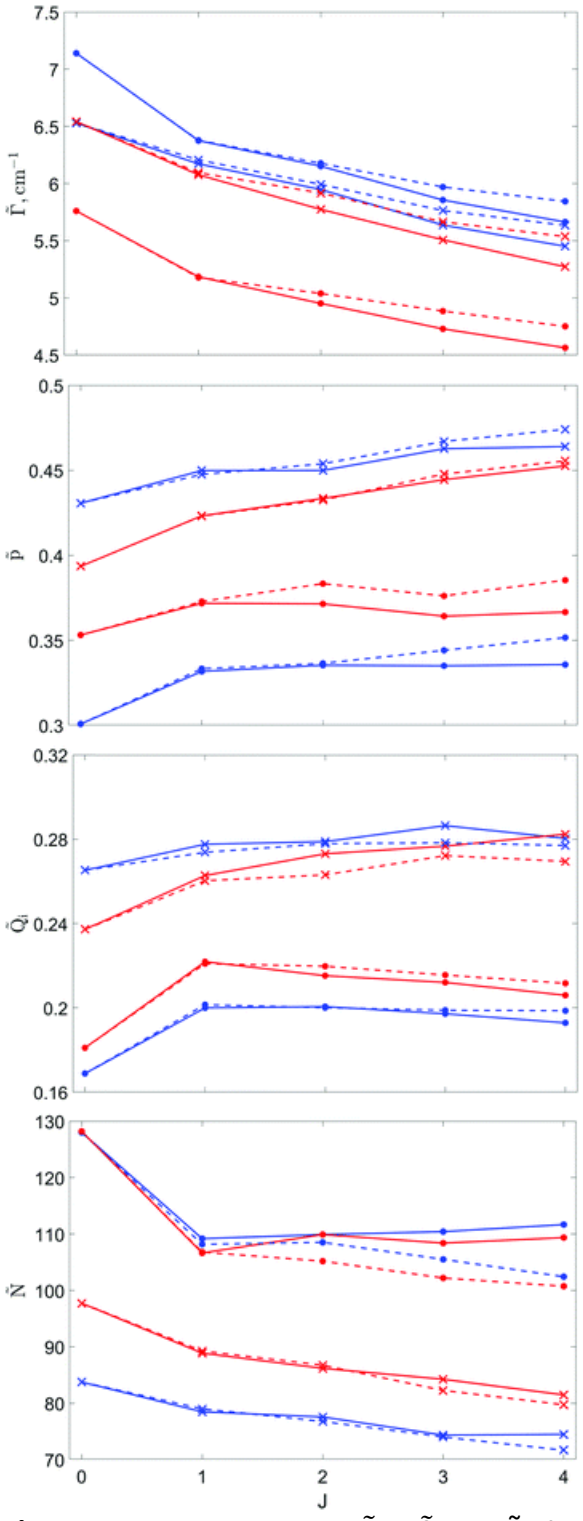

Fig. 4 The average properties $\tilde{\Gamma}, \tilde{p}, \tilde{Q}_i$ and $\tilde{N}$ of scattering resonances in ozone (see text) as a function of rotational excitation up to $J = 4$. States localized over the covalent well, and those distributed over the van der Waals region of the PES, are both included. The blue (red) color corresponds to the singly (doubly) substituted isotopologues of ozone. The dots (×-symbols) correspond to symmetric (asymmetric) isotopomers. The solid (dashed) lines correspond to the accurate coupled rotation–vibration (approximate symmetric-top rotor) calculations.

IV. Discussion

A. Implications for symmetry-driven isotope effect

Recombination reaction that forms ozone exhibits a robust symmetry-driven isotope effect, namely, in the experiment[9] the asymmetric ozone molecules (such as $^{16}O^{16}O^{18}O$ and $^{16}O^{18}O^{18}O$) are formed at a rate that is about 16% higher than the rate of formation of symmetric ozone molecules (such as $^{16}O^{16}O^{16}O$, $^{16}O^{18}O^{16}O$ or $^{18}O\ ^{16}O^{18}O$). This interesting phenomenon is an old mystery in the chemical physics and in the field of atmospheric and geochemistry too.[2,34] It is sometimes argued in the literature[4,37] that this effect can be explained if one assumes (and proves) that the symmetric and asymmetric ozone molecules possess different lifetimes. Let us review the data in Tables 2–4 in the light of this hypothesis.

To begin with, one should keep in mind that the rate of ozone recombination is determined by the dynamical partition function of scattering resonances Q, rather than by $\tilde{\Gamma}$ directly. The dependence of Q on the values of Γ_i of individual resonances is given by their weights w_i in eqn (13) above.

With the choice of $[\mathrm{M}] = 0.3$ Bar, the value of weight $w_i = 0.5$ corresponds to $\Gamma_i \approx 8 \times 10^{-3}$ cm^{-1}, while the values of w_i = 0.1 and 0.9 correspond to $\Gamma_i \approx 9 \times 10^{-4}$ and 7×10^{-2} cm^{-1}, respectively. For practical purposes, all resonances with Γ_i > 1 cm^{-1} can be considered as broad, which means that their weight w_i at a given pressure reached the maximum (w_i = 1) and thus it does not depend on the actual value of Γ_i anymore.

With this in mind, let us review the results of Table 2 first, for resonances localized over the covalent wells. We see that indeed the asymmetric ozone molecules $^{16}O^{16}O^{18}O$ and $^{16}O^{18}O^{18}O$ exhibit larger values of $\tilde{\Gamma}$ and one may (erroneously) expect that those would translate into larger values of weights w_i and partition functions Q (and thus higher rates of recombination). However, the values of Q in Table 2 show an opposite trend, they are smaller for the asymmetric molecules, compared to the symmetric ones. How can that be? Well, notice that the values of average $\tilde{\Gamma}$ reported in the Table 2 are in the range of broad resonances, when the actual values of resonance widths do not affect the recombination process anymore (even if they show some mass-independent symmetry-driven trend). Therefore, a property other than the resonance width Γ_i must be important for explanation of the trends of Q values seen in Table 2.

Let us consider the quantities in rows 3–6 of Tables 2–4. All these quantities are weighted averages, which take into account the contribution Q_i of each state (its importance). From these data it becomes very clear that the values of partition function Q correlate well with the average number of resonances $\tilde{N}$, rather than with the average resonance width $\tilde{\Gamma}$, which means that the main driver of the effect is the number of metastable states in the symmetric and asymmetric ozone molecules (not their lifetimes). And, it appears that asymmetric ozone molecules have smaller number of states $\tilde{N}$, compared to the symmetric ozone molecules, just opposite to what we hoped to find (beyond the factor of 2, applied to the values of Q for asymmetric isotopomers, as stated above).

The symmetry-driven isotope effect itself, can be expressed as a ratio of partition functions for asymmetric and symmetric molecules. In the experiments of Mauersberger group[9] these numbers were found to be on the order of $\eta = 1.16$ or so. Last row of Tables 2 and 4 reports our data for η, based on the calculations for $0 \leq \mathrm{J} \leq 4$ combined. The dependence of isotope effect on rotational

excitation, $\eta(J)$, is presented in Fig. S3 of the ESI.† Unfortunately, neither of these data come close to the experimental results. Indeed, if only the resonances localized over the covalent well are considered, then we obtain $\eta < 1$ (last row in Table 2), for both singly and doubly substituted cases, while in the experiment the isotope effect is observed to occur in the opposite direction, $\eta > 1$.

B. The effect of van der Waals states

Table 3 contains the same analysis, but for the scattering resonances distributed over the vdW parts of the PES: the weighted average values of $\tilde{p}$, $\tilde{Q}_i$, $\tilde{N}$ (see Fig. S5–S7 in the ESI† for their dependencies on the rotational excitation J). Table 4 and Fig. 4 contain the data $\tilde{p}$, $\tilde{Q}_i$, $\tilde{N}$ and η, obtained when the contribution of vdW states is added to the covalent well states. Since the partition functions Q of the vdW states are larger than those of the covalent-well states, it is not surprising that many properties listed in Table 4 are dominated by those listed in Table 3. Interestingly, the overall average number of resonances $\tilde{N}$ (in Table 4) is still smaller for asymmetric ozone molecules, in both singly and doubly substituted cases. This feature can be (at least partially) explained by the fact that for the highly delocalized states probability in the asymmetric region of PES is expected to be roughly twice as large compared to the symmetric region (see Fig. 1). This contributes to higher values of $\tilde{p}$ and $\tilde{Q}_i$ for asymmetric isotopomers and eventually translates to lower values of $\tilde{N}$.

These differences, although mass-independent, have no influence on the isotope effect, which depends on the values of Q only. Importantly, the isotope effect η vanishes almost entirely when all ozone states are taken together, in both cases of single and double isotopic substitutions (last row in Table 4). Fig. 5 represents evolution of the corresponding isotope effect, $\eta(J)$, as rotational excitation is raised. Here we can see some progressive deviation from the reference value of $\eta = 1$ (which corresponds to no isotope effect), but it is rather small and occurs in the opposite directions for singly and doubly substituted ozone molecules, which is consistent with our earlier findings for the bound states of ozone,[17] but is inconsistent with experimental data, where the same value of η is found irrespectively of the number of isotopic substitutions.

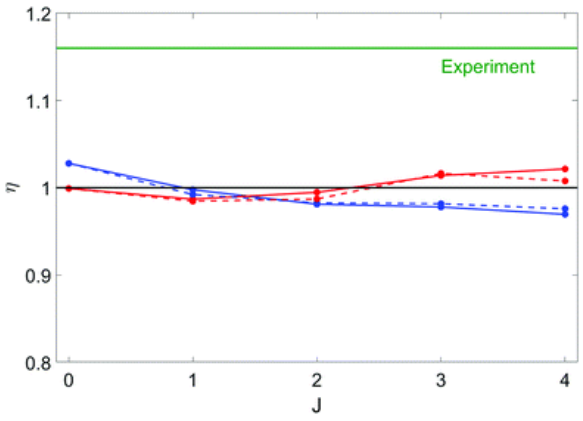

Fig. 5 Symmetry driven isotope effect η in ozone as a function of rotational excitation up to $J = 4$. States localized over the covalent well, and those distributed over the van der Waals region of the PES, are both included. The blue (red) color corresponds to the singly (doubly) substituted isotopologues of ozone. The solid (dashed) lines correspond to the accurate coupled rotation–vibration (approximate symmetric-top rotor) calculations.

It is quite unfortunate but based on the data obtained here for a limited range of rotational excitations $0 \leq J \leq 4$, we cannot come out with any reliable explanation of large and robust η-effect observed in the experiments.

C. The influence of rotation–vibration coupling (Coriolis effect)

One of the main goals of this paper was to check whether the symmetry-driven isotope effect could be explained by the Coriolis coupling which, according to a recently published hypothesis,[11] may act differently in symmetric and asymmetric ozone molecules. All results presented and discussed so far were obtained using an accurate (basically exact) coupled rotational–vibrational calculations, which include the asymmetric-top rotor term and the Coriolis coupling term in the Hamiltonian, see the last line of eqn (10). Such calculations are numerically demanding. In addition, we carried out a set of approximate calculations neglecting these rotation–vibration coupling terms, which corresponds to a symmetric-top rotor approximation (Λ is assumed to be a good quantum number). Such calculations are much cheaper, since different Λ-blocks of the Hamiltonian matrix are uncoupled, and thus can be diagonalized independently. The results of these simplified calculations are also presented in Tables 1–4 (in parentheses), in Fig. 3–5 in the main text and in Fig. S1–S6 of the ESI† (dashed-lines).

Without going through comparison of each pair of numbers, let us summarize what we learned about the role of rotation–vibration coupling (interested readers are invited to look through all data):

(1) We found that the values of Q, $\tilde{\Gamma}$ and $\tilde{N}$ are indeed somewhat affected by inclusion of the rotation–vibration coupling, but these changes are almost uniform across isotopomers, so, none of the computed properties change their relative order.

(2) Therefore, the value of isotope effect η remains nearly the same for both singly and doubly substituted ozone molecules, in both Table 2 (only resonances localized over the covalent well) and Table 4 (vdW states added to the covalent ones).

(3) The values of Q and $\tilde{N}$ always increase as the rotation–vibration coupling is included, which indicates that on average the spectrum of the uncoupled ozone states is less dense, as one might expect.

(4) In contrast, the values of $\tilde{\Gamma}$ always decrease, which indicates that on average the resonances are made more stable by inclusion of the rotation–vibration coupling, they live longer, decay slower.

(5) The change is slightly larger for resonances localized over the covalent well, than for the vdW states, presumably because the stretched vdW complexes are closer to the symmetric-top rotor model, than their compact covalently bound counterparts.

Moreover, from Fig. 3 we see that at larger values of J the effect of rotation–vibration coupling on the magnitude of the partition function Q grows roughly linearly with J. However, from Fig. 5 we see that the influence of rotation–vibration coupling on the value of isotope effect η, which is the ratio of Q for asymmetric and symmetric ozone molecules, remains small through the range of J values considered here.

Based on these data we can conclude that the Coriolis effect (rotational–vibrational coupling) influences symmetric and asymmetric ozone molecules in a similar way, and largely cancels if the ratio of partition functions is computed.

V. Conclusions

In this work we developed a method that permits to carry out, in a cost-efficient way, accurate variational calculations of coupled rotation–vibration states for a broad range of rotational excitations of a molecule. Such calculations are required when we want to predict thermal rate of a reaction, or another property (such as partition function) averaged over a broad distribution of the rotational excitations. Traditional approach is to use multiple vibrational basis sets, optimized and truncated for each individual rotational state. This is elegant but is numerically inefficient. We demonstrated here that it is possible to choose one vibrational basis set, optimized for a typical rotational excitation (J, Λ), say somewhere in the middle of the desired range of rotational excitations, to employ it in the coupled rotation–vibration calculations for many values of J, in a relatively broad range.

This method is implemented in the SpectrumSDT program for calculation of the coupled rotation–vibration spectra of triatomic molecules using hyper-spherical coordinates. The new code is tested by computing the bound rotational–vibrational states of ozone available from literature. The new procedure is found to be very efficient and capable of expanding the range of the bound state calculations up to the rotational excitations with $J = 56$ (compared to $J = 5$ in the literature). The results of these bound state calculations will be reported elsewhere.

In this paper the goal was to reach higher vibrational energies, above dissociation threshold, to determine how the rotation–vibration coupling influences scattering resonances in ozone. These metastable states participate in the ozone forming reaction and their properties are believed to be responsible for the mass-independent symmetry-driven isotope effect. Not only the states localized in the compact covalent well of ozone, but also the large-amplitude states distributed over a broad vdW interaction plateau of the PES are of interest.

It should be emphasized that, for resonances above the dissociation threshold, using the traditional method and the earlier version of code we were only able to do the uncoupled rotation–vibration calculations for one value of (J, Λ) at a time (one Λ-block of the Hamiltonian matrix, uncoupled from all other Λ-blocks of this J). Even the calculations of scattering resonances with two coupled Λ-blocks (such as for $J = 1$ odd parity, or for $J = 2$ odd parity) were at the limit of our computing power. Using the new method and code, we are now able to carry out accurate coupled rotation–vibration calculations of scattering resonances in ozone with up to five coupled Λ-blocks ($J = 4$ even parity). While these data are still insufficient for prediction of thermal rates at room temperature, they start giving us some accurate and thus valuable information about the influence of rotation–vibration coupling (the Coriolis force) on the recombination reaction of ozone, and on the corresponding isotope effect. This was not available in the past.

Analysis of our data indicates that the average properties of scattering resonances, such as their average lifetime $\tilde{\Gamma}$, the average number of such states $\tilde{N}$, and their cumulative partition function Q, are all affected by the rotation–vibration coupling, and this effect grows as the value of angular momentum J is increased. However, we also found that various isotopomers and isotopologues of

ozone (symmetric and asymmetric ozone molecules with single and double isotopic substitutions) are influenced by the Coriolis effect rather uniformly. When the ratio η of partition functions for asymmetric *vs*. symmetric ozone molecules is computed, the Coriolis effect largely cancels, and this cancelation seems to occur for all values of J. So far, we were not able to attribute any appreciable mass-independent symmetry-driven isotopic fractionation to the Coriolis coupling effect.

If more computational resources become available, we should be able to extend the range of covered J values up to probably $J = 10$, using this same methodology. For calculations of scattering resonances at even larger values of the rotational excitation J one may need to use other tricks.

Data availability statement

The data that supports the findings of this study are available within the article and its ESI.†

Conflicts of interest

There are no conflicts to declare.

Acknowledgements

This research was supported by the NSF AGS program Grant No. AGS-1920523. We used resources of the National Energy Research Scientific Computing Center, which is supported by the Office of Science of the U.S. Department of Energy under Contract No. DE-AC02-5CH11231. Igor Gayday acknowledges the support of Schmitt Fellowship and MolSSI Investment Fellowship. MolSSI Investment Fellowship is supported by NSF ACI-1547580. Richard Dawes is gratefully acknowledged for sharing the PES of ozone. Jose E. Roman is gratefully acknowledged for his advices regarding the use of SLEPc library. Alexander Teplukhin is gratefully acknowledged for fruitful discussions.

References

1. K. Mauersberger Measurement of heavy ozone in the stratosphere, *Geophys. Res. Lett.*, 1981, **8** , 935 —937.
2. M. H. Thiemens and J. E. Heidenreich , The Mass-Independent Fractionation of Oxygen: A Novel Isotope Effect and Its Possible Cosmochemical Implications, *Science*, 1983, **219** , 1073 —1075.
3. D. Babikov , B. K. Kendrick , R. B. Walker , R. T. Pack , P. Fleurat-Lessard and R. Schinke , Formation of ozone: Metastable states and anomalous isotope effect, *J. Chem. Phys.*, 2003, **119** , 2577 —2589.
4. P. Reinhardt and F. Robert , On the mass independent isotope fractionation in ozone, *Chem. Phys.*, 2018, **513** , 287 —294.
5. Y. Q. Gao and R. A. Marcus , Strange and unconventional isotope effects in ozone formation, *Science*, 2001, **293** , 259 —263.
6. C. Janssen and R. A. Marcus , Does Symmetry Drive Isotopic Anomalies in Ozone Isotopomer Formation?, *Science*, 2001, **294** , 951a.
7. R. Schinke , S. Y. Grebenshchikov , M. V. Ivanov and P. Fleurat-Lessard , Dynamical Studies of the Ozone Isotope Effect: A Status Report, *Annu. Rev. Phys. Chem.*, 2006, **57** , 625 —661.
8. K. Mauersberger , D. Krankowsky , C. Janssen and R. Schinke , Assessment of the ozone isotope effect, *Adv. At., Mol., Opt. Phys.*, 2005, **50** , 1 —54.

9. C. Janssen , J. Guenther , K. Mauersberger and D. Krankowsky , Kinetic origin of the ozone isotope effect: a critical analysis of enrichments and rate coefficients, *Phys. Chem. Chem. Phys.*, 2001, **3** , 4718 —4721.
10. M. Kryvohuz and R. A. Marcus , Coriolis coupling as a source of non-RRKM effects in ozone molecule: Lifetime statistics of vibrationally excited ozone molecules, *J. Chem. Phys.*, 2010, **132** , 224305.
11. M. Kryvohuz and R. A. Marcus , Coriolis coupling as a source of non-RRKM effects in triatomic near-symmetric top molecules: Diffusive intramolecular energy exchange between rotational and vibrational degrees of freedom, *J. Chem. Phys.*, 2010, **132** , 224304.
12. A. Barbe , S. Mikhailenko , E. Starikova , M.-R. De Backer , V. G. Tyuterev and D. Mondelain , *et al.*, Ozone spectroscopy in the electronic ground state: High-resolution spectra analyses and update of line parameters since 2003, *J. Quant. Spectrosc. Radiat. Transfer*, 2013, 172 —190.
13. A. Barbe , E. Starikova , M. R. De Backer and V. G. Tyuterev , Analyses of infrared FT spectra of asymmetric ozone isotopologue $^{16}O^{16}O^{18}O$ in the range 950–3850 cm^{-1}, *J. Quant. Spectrosc. Radiat. Transfer*, 2018, **218** , 231 —247.
14. I. Gayday , A. Teplukhin and D. Babikov , The ratio of the number of states in asymmetric and symmetric ozone molecules deviates from the statistical value of 2, *J. Chem. Phys.*, 2019, **150** , 101104.
15. V. Kokoouline , D. Lapierre , A. Alijah and V. G. Tyuterev , Localized and delocalized bound states of the main isotopologue $^{48}O_3$ and of ^{18}O-enriched $^{50}O_3$ isotopomers of the ozone molecule near the dissociation threshold, *Phys. Chem. Chem. Phys.*, 2020, **22** , 15885 —15899.
16. I. Gayday , A. Teplukhin , B. K. Kendrick and D. Babikov , Theoretical Treatment of the Coriolis Effect Using Hyperspherical Coordinates, with Application to the Ro-Vibrational Spectrum of Ozone, *J. Phys. Chem. A*, 2020, **124** , 2808 —2819.
17. I. Gayday , A. Teplukhin , B. K. Kendrick and D. Babikov , The role of rotation–vibration coupling in symmetric and asymmetric isotopomers of ozone, *J. Chem. Phys.*, 2020, **152** , 144104.
18. D. Charlo and D. C. Clary , Quantum-mechanical calculations on termolecular association reactions XY + Z + M → XYZ + M: Application to ozone formation, *J. Chem. Phys.*, 2002, **117** , 1660 —1672.
19. D. Charlo and D. C. Clary , Quantum-mechanical calculations on pressure and temperature dependence of three-body recombination reactions: Application to ozone formation rates, *J. Chem. Phys.*, 2004, **120** , 2700 —2707.
20. T. Xie and J. M. Bowman , Quantum inelastic scattering study of isotope effects in ozone stabilization dynamics, *Chem. Phys. Lett.*, 2005, **412** , 131 —134.
21. S. Y. Grebenshchikov and R. Schinke , Towards quantum mechanical description of the unconventional mass-dependent isotope effect in ozone: Resonance recombination in the strong collision approximation, *J. Chem. Phys.*, 2009, **131** , 181103.
22. A. Teplukhin and D. Babikov , Efficient method for calculations of ro-vibrational states in triatomic molecules near dissociation threshold: Application to ozone, *J. Chem. Phys.*, 2016, **145** , 114106.
23. A. Teplukhin , I. Gayday and D. Babikov , Several levels of theory for description of isotope effects in ozone: Effect of resonance lifetimes and channel couplings, *J. Chem. Phys.*, 2018, **149** , 164302.

24. C. Petty , R. F. K. Spada , F. B. C. Machado and B. Poirier , Accurate rovibrational energies of ozone isotopologues up to J = 10 utilizing artificial neural networks, *J. Chem. Phys.*, 2018, **149** , 024307.
25. C. Leforestier Grid representation of rotating triatomics, *J. Chem. Phys.*, 1991, **94** , 6388 —6397.
26. J. M. Launay and M. Le Dourneuf , Hyperspherical close-coupling calculation of integral cross sections for the reaction H + H_2 → H_2 + H, *Chem. Phys. Lett.*, 1989, **163** , 178 —188.
27. V. Hernandez , J. E. Roman and V. Vidal , SLEPc: A Scalable and Flexible Toolkit for the Solution of Eigenvalue Problems, *ACM Trans. Math. Softw.*, 2005, **31** , 351 —362.
28. V. Hernández , J. E. Román and V. Vidal , SLEPc: Scalable Library for Eigenvalue Problem Computations, *Lecture Notes in Computer Science* , Springer, 2003, pp. 377–391.
29. V. Hernandez , J. E. Roman and A. Tomas , Parallel Arnoldi eigensolvers with enhanced scalability via global communications rearrangement, *Parallel Comput.*, 2007, **33** , 521 —540.
30. D. E. Manolopoulos Derivation and reflection properties of a transmission-free absorbing potential, *J. Chem. Phys.*, 2002, **117** , 9552 —9559.
31. S. A. Ndengué , R. Dawes , X.-G. Wang , T. Carrington , Z. Sun and H. Guo , Calculated vibrational states of ozone up to dissociation, *J. Chem. Phys.*, 2016, **144** , 074302.
32. V. G. Tyuterev , R. V. Kochanov , S. A. Tashkun , F. Holka and P. G. Szalay , New analytical model for the ozone electronic ground state potential surface and accurate ab initio vibrational predictions at high energy range, *J. Chem. Phys.*, 2013, **139** , 134307.
33. P. Honvault , G. Guillon , R. Kochanov and V. Tyuterev , Quantum mechanical study of the ^{16}O + $^{18}O^{18}O$ → $^{16}O^{18}O$ + ^{18}O exchange reaction: Integral cross sections and rate constants, *J. Chem. Phys.*, 2018, **149** , 214304.
34. J. Morton , J. Barnes , B. Schueler and K. Mauersberger , Laboratory studies of heavy ozone, *J. Geophys. Res.*, 1990, **95** , 901.
35. S. Y. Grebenshchikov , R. Schinke , P. Fleurat-Lessard and M. Joyeux , van der Waals states in ozone and their influence on the threshold spectrum of $O_3(X^1A_1)$. I. Bound states, *J. Chem. Phys.*, 2003, **119** , 6512 —6523.
36. M. V. Ivanov and D. Babikov , Collisional stabilization of van der Waals states of ozone, *J. Chem. Phys.*, 2011, **134** , 174308.
37. F. Robert , L. Baraut-Guinet , P. Cartigny and P. Reinhardt , An experimental test for the mass independent isotopic fractionation mechanism proposed for ozone, *Chem. Phys.*, 2019, **523** , 191 —197.

Footnote

† Electronic supplementary information (ESI) available: Section A contains all technical details of calculations. Section B provides analogues of Fig. 1 and Table 1 for the doubly substituted case. Sections C and D provide the sets of figures for *J*-dependent properties of the covalent and the VdW states, separately, analogous to Fig. 3–5 of the main text. Also, an archive file is provided with raw outputs of SpectrumSDT, containing all spectra of ozone used in this work (both bound and resonance states) and their properties. This is described in Section E. See DOI: 10.1039/d0cp05060a